ACS chemical biology

Articles

pubs.acs.org/acschemicalbiology

Identification and Characterization of a Multifunctional Dye Peroxidase from a Lignin-Reactive Bacterium

Margaret E. Brown,[†] Tiago Barros,[§] and Michelle C. Y. Chang*[,†,‡]

[†]Department of Chemistry, [‡]Department of Molecular and Cell Biology, and [§]Howard Hughes Medical Institute, University of California, Berkeley, California 94720-1460, United States

Supporting Information

ABSTRACT: Plant biomass represents a renewable feedstock that has not yet been fully tapped because of the difficulty in accessing the carbon in its structural biopolymers. Lignin is an especially challenging substrate, but select microbes have evolved complex systems of enzymes for its breakdown through a radical-mediated oxidation process. Fungal systems are well-characterized for their ability to depolymerize lignin, but the ability of bacteria to react with this substrate remains elusive. We have therefore focused on elucidating strategies used by lignin-reactive soil bacteria and describing their oxidative enzyme systems. We now report the identification and characterization of an unusual C-type dye-decolorizing peroxidase from *Amycolatopsis* sp. 75iv2 (DyP2), which belongs to a family of heme peroxidases reported to be involved in bacterial lignin degradation. Biochemical studies indicate that DyP2 has novel function for this family, with versatile and high activity both as a peroxidase and Mn peroxidase ($k_{cat}/K_M \approx 10^5-10^6$ M^{-1} s^{-1}). It also has a Mn-dependent oxidase mode of action that expands its substrate scope. Crystallographic studies of DyP2 at 2.25 Å resolution show the existence of a Mn binding pocket and support its key role in catalysis.

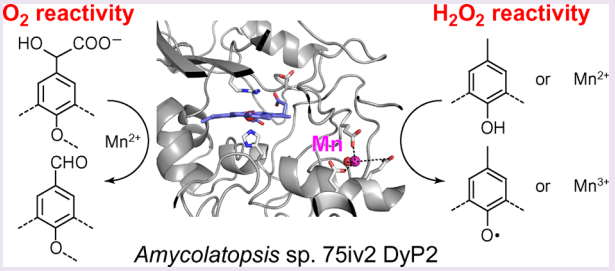

The large-scale production of fine and commodity chemicals forms the basis for modern society yet relies almost completely on petroleum-derived feedstocks as a carbon source. One of the few alternative resources that is produced in high enough volume to displace a significant level of fossil fuels is plant biomass, which is both renewable and has the potential to provide carbon on the order of 10−50 billion tons per year.[1,2] Although sugars, starches, and oils have entered the pipeline, the majority of plant material is made up of structural biopolymers that are resistant to processing and downstream utilization for chemical and biological processes.[3,4] Of these, lignin perhaps requires the most challenging chemistry for its degradation as it is a highly cross-linked aromatic polymer containing a wide variety of C−C and C−O bonding motifs.[5] Despite its recalcitrance, select microbes have evolved the ability to react with and depolymerize lignin. Our group is interested in studying the biochemical logic underlying the transformation of complex substrates by living organisms with the overall goal of elucidating new molecular strategies for lignin degradation.

Fungal systems have been well-characterized both *in vivo* and *in vitro* to be highly active for lignin depolymerization, using families of heme- and multicopper-dependent oxidative enzymes to carry out radical-mediated degradation.[6,7] In comparison, bacterial systems are less well understood with regard to lignin reactivity and thus represent an interesting area for exploring the diversity of enzymatic strategies for biomass deconstruction.[8−10] Many soil bacteria have been reported to modify lignin to produce acid-precipitable polymeric lignin (APPL),[11] which is a different product than produced from fungal activity. Of these, *Amycolatopsis* sp. 75iv2 demonstrates particularly high capacity with regard to both production of APPL as well as extracellular phenol oxidation capacity.[12]

We have set out to characterize the oxidative system of *A.* sp. 75iv2, which includes a large set of heme peroxidases and multicopper laccases.[12,13] Interestingly, genome mining reveals that *A.* sp. 75iv2 also contains three genes encoding dye-decolorizing peroxidases (DyPs), which are a relatively small but distinct class of heme peroxidases that are often involved in the extracellular degradation of aromatics.[14−20] More recently, DyPs have been implicated in bacterial lignin degradation in the soil bacterium, *Rhodococcus jostii* RHA1.[21,22] We now report the biochemical and structural characterization of an unusual DyP from *A.* sp. 75iv2 (DyP2) that has both high peroxidase and manganese peroxidase activity. Furthermore, it has a second mode of oxidase reactivity that expands its substrate range.

RESULTS AND DISCUSSION

Phylogenetic Analysis of the DyPs from *A.* sp. 75iv2. DyPs can be classified according to four different clades. In general, DyPs from bacteria are smaller in size and fall within the A- and B-clades, whereas fungal enzymes are typically found to cluster within the D-clade.[18,22] A DyP phylogenetic tree was

Received: July 24, 2012
Accepted: September 27, 2012
Published: October 10, 2012

constructed by searching the UniRef50 database using structurally characterized DyPs that represent each clade to obtain sequences with <50% identity. Phylogenetic analysis of the DyPs from *A.* sp. 75iv2 indicates that two belong to the C-clade (DyP1−2), which are clustered away from most prokaryotic DyPs but are related to fungal D-type DyPs (Figure 1, Supplementary Figure S1). Interestingly, many of the

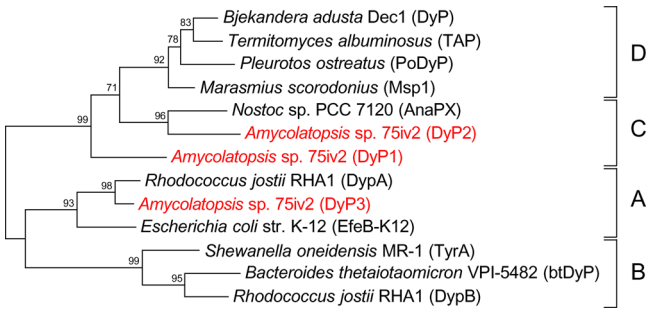

Figure 1. Compressed phylogenetic tree comparing DyP1−3 (red) from *A.* sp. 75iv2 with structurally and/or biochemically characterized DyPs. Bootstrap values are indicated at branchpoints.

other C-type DyPs belong to related actinomycetes that have also been reported to produce APPL and can be found clustered in the genome with biomass-processing enzymes (Supplementary Table S2, Figure S2). However, DyP2 belongs to an especially divergent and sparsely populated branch of the C-clade. Consequently, additional DyP2 homologues were identified by BLAST to fill this branch and were found to consist of only a handful of sequences that mostly originate from cyanobacteria (Supplementary Figure S1, Table S2). The third DyP from *A.* sp. 75iv2, DyP3, can be grouped with other canonical bacterial DyPs, such as the one found to be partially responsible for the lignolytic behavior of *R. jostii* RHA1.[21,22]

Biochemical Characterization of the C-type DyP2 from *A.* sp. 75iv2. On the basis of its unusual phylogeny and the sequence context of other C-type DyPs from lignin-reactive actinomycetes, we cloned and heterologously expressed DyP2 from *A.* sp. 75iv2 with an N-terminal His_{10}-tag containing a linker with a Tobacco Etch Virus (TEV) protease site in *Escherichia coli* (Supplementary Figure S3). After nickel affinity chromatography, the DyP2 protein was characterized by size-exclusion chromatography (SEC) and observed to exist both as a monomeric and oligomeric species (n = 4−6) in solution (Supplementary Figure S3). Further analysis showed that the monomeric form contained no bound heme cofactor, and its removal by SEC significantly increased the specific activity of DyP2. After SEC, it appeared as if a bound imidazole remained associated with the heme cofactor by UV−vis spectroscopy (Supplementary Figure S3). Consequently, DyP2 was dialyzed until the λ_{max} of the Soret band blue-shifted into the expected range for a high-spin Fe^{3+}-hemoprotein with a proximal histidine ($\lambda_{max} \approx$ 400−410 nm). The introduction of these two steps to the purification of DyP2 increased the peroxidase activity of DyP2 by 3,500-fold compared to the enzyme as directly isolated after affinity chromatography. Using a combination of inductively coupled plasma-optical emission spectroscopy (ICP-OES) and protein acidolysis, the heme occupancy of the purified DyP2 was determined to be >99% (Supplementary Figure S4). Since removal of the His_{10}-tag by cleavage at the intervening TEV protease site did not appear to

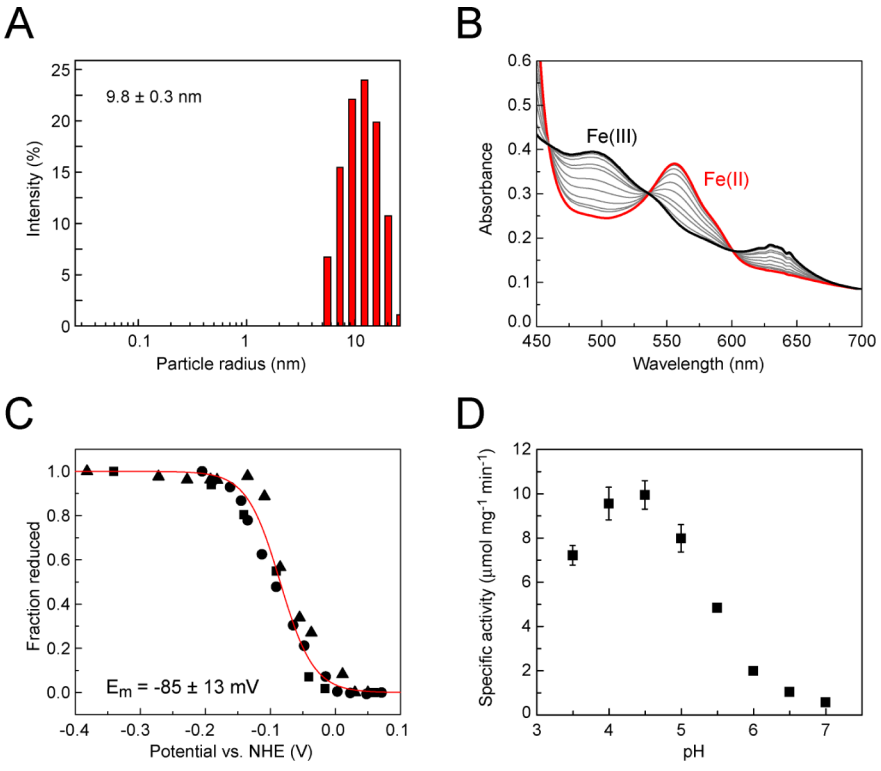

Figure 2. Biochemical characterization of DyP2 from *A.* sp. 75iv2. (A) Dynamic light scattering measurements of DyP2 in 20 mM Tris, 50 mM KCl, pH 7.5 indicate that its size in solution is consistent with an oligomer. (B) Changes in the electron absorption spectrum showing the stepwise oxidation of Fe^{2+}-DyP2 (red) to Fe^{3+}-DyP2 (black). (C) Three individual redox titrations of DyP2 monitored by $\Delta A_{560\ nm}$. (D) pH−rate profile for the H_2O_2-dependent oxidation of Reactive Blue 5 by DyP2. Data are reported as mean ± SD.

dx.doi.org/10.1021/cb300383y | *ACS Chem. Biol.* 2012, 7, 2074−2081

Table 1. Peroxidase and Mn Peroxidase Activity of DyP2[a]

			k_{cat}/K_M (M^{-1} s^{-1})			
Clade	Protein	Source	ABTS	Reactive Blue 5	Reactive Black 5	Mn^{2+}
A	DypA[21]	*Rhodococcus jostii* RHA1	$(2.0 \pm 0.1) \times 10^3$			ND
B	DypB[21]	*Rhodococcus jostii* RHA1	$(2.4 \pm 0.1) \times 10^3$			$(2.5 \pm 0.01) \times 10^1$
	DyPPa[20]	*Pseudomonas aeruginosa*		2.2×10^2		
	TyrA[29]	*Shewanella oneidensis*		7.0×10^4		
C	**DyP2**	***Amycolatopsis* sp. 75iv2**	$\mathbf{(6.6 \pm 0.9) \times 10^6}$	$\mathbf{(7.1 \pm 0.9) \times 10^5}$	$\mathbf{(1.6 \pm 0.1) \times 10^5}$	$\mathbf{(1.2 \pm 0.2) \times 10^5}$
	AnaPX[18]	*Nostoc* sp. PCC 7120		1.2×10^7		ND
D	DyP[23]	*Bjerkandera adusta* Dec1		4.8×10^6		
	AjP I[19]	*Auricularia auricula-judae*	1.8×10^7	5.0×10^6	5.7×10^5	ND
	AjP II[19]	*Auricularia auricula-judae*	1.6×10^7	1.7×10^7	4.1×10^5	ND
	TAP[15]	*Termitomyces albuminosus*	2.5×10^7			ND
Other	LiP[30]	*Phanerochaete chrysosporium*	$(5.6 \pm 0.4) \times 10^5$		ND	ND
	MnP[28,31]	*Phanerochaete chrysosporium*	ND		ND	$(1.2 \pm 0.1) \times 10^7$
	VP[32]	*Pleurotus eryngii*	$(9.4 \pm 0.8) \times 10^6$		$(1.7 \pm 0.1) \times 10^6$	$(1.8 \pm 0.1) \times 10^6$

[a]Comparison of DyP2 k_{cat}/K_M's with other characterized DyPs[15,18−21,23] and canonical fungal peroxidases[28,30−32] involved in lignin degradation. (ND, not detected; blank, not determined)

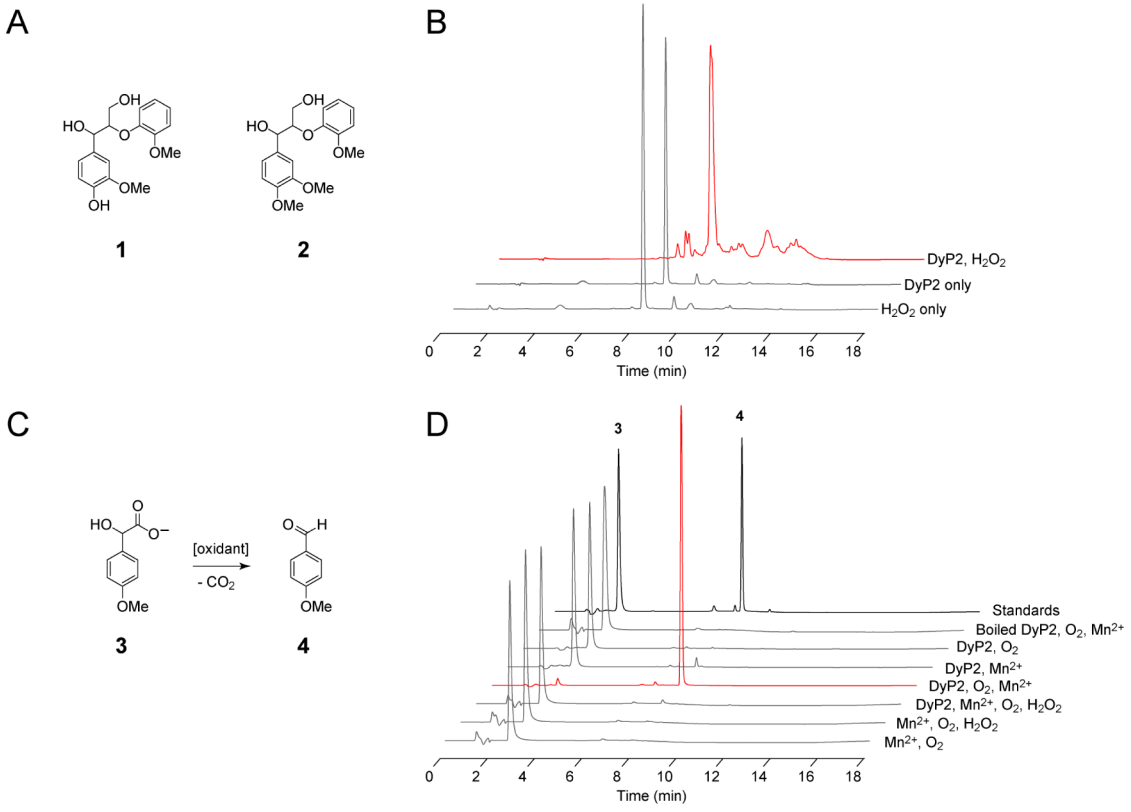

Figure 3. Peroxidase and oxidase reactivity of DyP2 from *A.* sp. 75iv2. (A) Model lignin dimers **1** and **2**. (B) HPLC traces showing the degradation of phenolic lignin model dimer **1** by DyP2 peroxidase activity monitored at $A_{254\ nm}$. (C) Oxidative decarboxylation of 4-methoxymandelic acid (**3**) to anisaldehyde (**4**). (D) HPLC traces showing the O_2- and Mn-dependent production of **4** catalyzed by DyP2 monitored by $A_{247\ nm}$.

change the oligomeric state by SEC or increase specific activity (Supplementary Figure S5), our biochemical and structural studies were carried out on His_{10}-DyP2.

In the DyP family, both monomeric[15,16,23] and oligomeric[15,17,18,20,24] members have been reported. Dynamic light scattering experiments were carried out to further characterize the oligomeric state of the active DyP2 enzyme in solution (Figure 2A, Supplementary Figure S6). The measured hydrodynamic radius is consistent with a solution state that is larger than a monomer based on the range of sizes observed for structurally characterized DyPs.[21,24,25] Additional characterization of purified DyP2 by UV−vis spectroscopy indicates that DyP2 is isolated in a high-spin Fe^{3+} resting state (Supplementary Figure S3). The Fe^{3+}/Fe^{2+} midpoint reduction potential was measured both by spectrochemical and spectroelectrochemical titration to be −85 ± 13 mV *vs* NHE with Nernstian behavior (Figure 2B,C). Although this potential is more positive than many typical heme peroxidases (−120 to −320 mV), it is close to that observed for manganese peroxidases.[26] In addition to biochemical characterization, we also analyzed the DyP2 sequence for canonical signal sequences for protein secretion, which are commonly found in enzymes

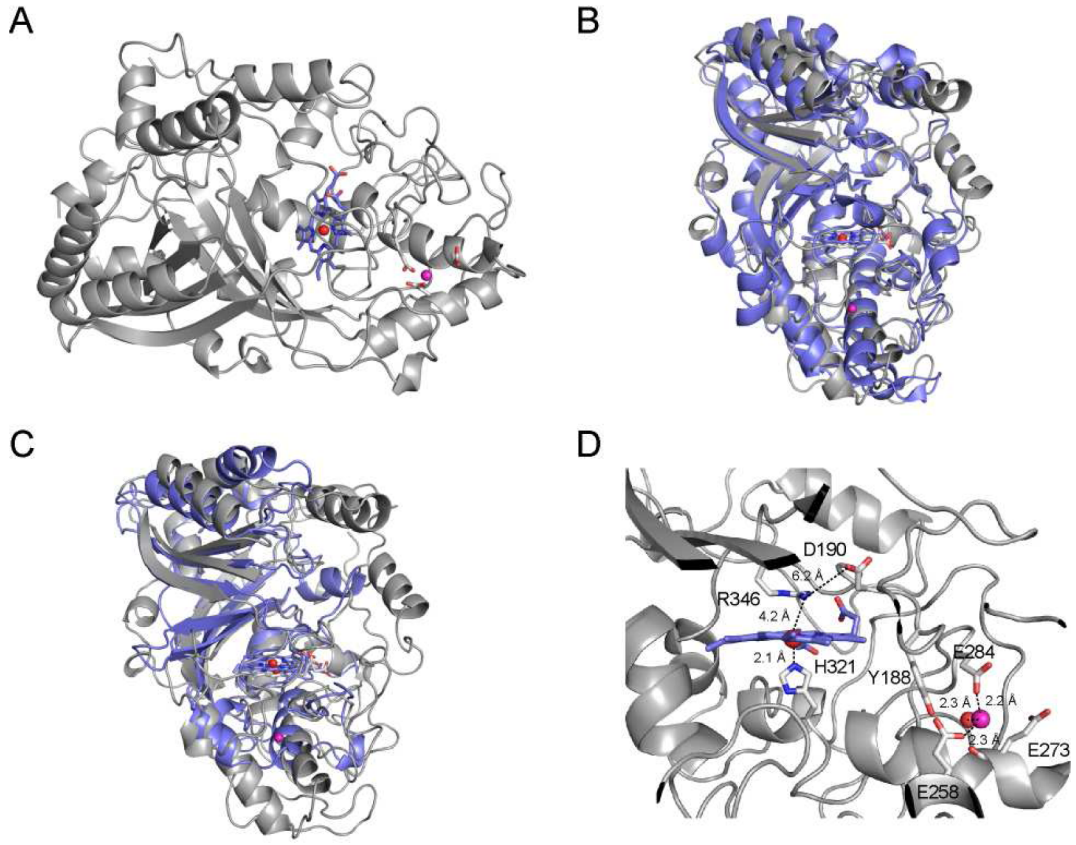

Figure 4. Structure of DyP2 from *A.* sp. 7Siv2. (A) Ribbon representation of DyP2 showing the overall fold of a DyP2 monomer and the heme site (Fe, red) and bound Mn ion (magenta), which are 15 Å apart. (B) Structural overlay of one DyP2 monomer (gray) with the D-type *B. adusta* Dec1 DyP (blue, PDB ID 2D3Q, 28% sequence identity) shows an RMSD of 2.7 Å for 417 aligned C_α atoms. (C) Structural overlay of one DyP2 monomer (gray) with the B-type DypB from *R. jostii* RHA1 (blue, PDB ID 3QNR). (D) View of the DyP2 active site of DyP2 showing the proximal H321 and distal pocket residues, D190 and R346. A Mn binding site near to the heme active site (15 Å apart) is formed by E258, E273, E284, and a structured water held in place by the main chain carbonyl group of E273 (2.7 Å). E273 is also found in a second conformation where it is directly coordinated to the Mn ion (Supplementary Figure S16). The Y188 is also shown and is located 3.9 Å from the Mn ion and 4.8 Å from the heme site.

with extracellular function (Supplementary Figure S7). Although no signal sequence was found, the secretory machinery for actinomycetes is not fully characterized, and the low pH optimum for DyP2 (Figure 2D) along with the observation that many DyPs have been isolated from the secreted protein fraction[14,17,19,23] imply that DyP2 could still possibly play a role in extracellular oxidation chemistry.

DyP2 Displays Versatile Peroxidase Activity with a Broad Substrate Scope. In order to explore its substrate scope, DyP2 was tested against a panel of peroxidase substrates including aromatics, azo dyes, anthroquinone dyes, and Mn^{2+}. DyP2 was found to be highly active in phenol oxidation using a standard 2,4-dichlorophenol peroxidase assay (Supplementary Figure S8). An additional signature of DyPs is their ability to degrade anthroquinone (Reactive Blue 5) as well as azo (ABTS) dyes.[14,19,20,27] We therefore characterized DyP2 with respect to both classes of substrates and found high specific activity toward Reactive Blue 5 and ABTS, with k_{cat}/K_M values that are more similar to the C- and D-type DyPs compared to the significantly lower values observed in the characterized bacterial A- and B-type DyPs (Table 1, Supplementary Table S3). Furthermore, DyP2 was found to be competent for the decolorization of Reactive Black 5, an azo dye considered to have a high oxidation potential due to the smaller number of enzymes that have been shown to be able to degrade this molecule.[28] The ability of DyP2 to degrade lignin model dimers containing the β-O-4 linkage[33] was assayed with two model substrates with (**1**) or without (**2**) a phenolic site (Figure 3A,B). These studies showed that DyP2 could rapidly break down **1** in the absence of redox mediators, but that the lower-potential phenolic site (ΔE = 0.6−0.8 V *vs* NHE)[34] is required for this activity as no degradation of **2** was observed under the same conditions (Supplementary Figure S9).

However, the most interesting behavior of DyP2 with respect to substrate scope is its high Mn^{2+} oxidation capacity. By analogy to fungal systems, manganese peroxidase activity has been thought to be important for microbial lignin degradation, taking advantage of the high Mn content of wood to produce the Mn^{3+} oxidant.[7] Indeed, a low level of Mn peroxidase activity was observed in DypB from *R. jostii* RHA1.[21] We therefore tested DyP2 for its ability to oxidize Mn^{2+} to Mn^{3+} in the present of H_2O_2 and found a surprisingly high activity with a k_{cat}/K_M (k_{cat} = 24 ± 1 s^{-1}; K_M = 0.21 ± 0.03 mM) that is only 10-fold lower than that of the versatile peroxidase from *Pleurotus eryngii* and 100-fold lower than that of the Mn peroxidase from *Phanerochaete chrysosporium* (Table 1, Supplementary Table S3), which belongs to one of the most active lignolytic systems found to date. Although other heme-dependent peroxidases have been found to display this versatility,[32] it has not yet been observed in any of the characterized DyPs.

dx.doi.org/10.1021/cb300383y | *ACS Chem. Biol.* 2012, 7, 2074−2081

DyP2 Also Demonstrates Oxidase Reactivity. Since no apparent reaction of DyP2 was observed with the nonphenolic lignin dimer **2**, we turned our attention to another lignin peroxidase substrate, 4-methoxymandelic acid (MMA, **3**),[35] which can spontaneously decarboxylate upon ring oxidation and thereby increase the sensitivity for detecting these high potential oxidation events (ΔE > 1.4 V *vs* NHE)[36] that have been observed in fungal lignin breakdown pathways (Figure 3C). In this assay, we observe a low level of conversion of **3** into the anisaldehyde product (**4**) by DyP2 (Figure 3D). The identity of **4** was confirmed by extraction of the DyP2 reaction product into ethyl acetate followed by GC−MS analysis compared to an authentic standard (Supplementary Figure S10).

Further studies of this phenomenon have shown that this process is actually independent of added H_2O_2 and requires O_2 and Mn^{2+} instead (Figure 3D, Supplementary Figure S11). Indeed, the oxidative decarboxylation of **3** is catalyzed quantitatively by DyP2 in the presence of O_2 and Mn^{2+} alone. Controls omitting Mn^{2+} and O_2 show that both are required for the conversion of **3** to **4**. Further characterization of this reaction indicates that the pH maximum occurs around pH 5 and that the K_M for Mn^{2+} (0.76 ± 0.07 mM) is similar to that measured for the Mn peroxidase activity (Supplementary Table S3, Figure S11). Thus, in addition to a high and versatile peroxidase activity, DyP2 also has an oxidase mode that is dependent on Mn^{2+}. Interestingly, the addition of Mn^{2+} is insufficient to convert the Fe^{3+}-resting state of DyP2 to an Fe^{2+}-state (Supplementary Figure S12), which is classically competent to interact with O_2. Thus, a more complex catalytic cycle may be possible, similar to that described for other peroxidases.[37,38] More importantly, the oxidase mode of reactivity expands the substrate scope of DyP2 and allows for reaction with more difficult substrates either by direct oxidation or H atom abstraction.

Structural Characterization of DyP2 from *A.* sp. 75iv2. As the multiple reaction modes and high activity of DyP2 as a peroxidase, Mn peroxidase, and oxidase are exceptional for the DyP family, we next focused on structural studies to further elucidate its function. We crystallized DyP2 and solved its structure at 2.25 Å resolution by a combination of partial molecular replacement using the DyP from *Bjerkandera adusta* Dec1[25] and experimental phasing obtained from selenomethionine-labeled DyP2 crystals (Figure 4A, Supplementary Table S4). Two DyP2 monomers are present in the asymmetric unit as an apparent dimer (Supplementary Figure S13), which is smaller than the size measured in solution (Figure 2A, Supplementary Figure S3).

Although several DyPs are reported to be dimers,[17,20,24] the DyP2 dimer observed in crystals appears to be non-native and induced by crystallization conditions. Despite the large interface (970 Å^2 per monomer), the energy for dimer formation calculated by PISA[39] is small ($\Delta G \approx -0.6$ kcal/mol) and is stabilized mainly by solvent molecules and polar rather than hydrophobic interactions between the monomers (Supplementary Figure S13). Therefore, the DyP2 oligomer observed in solution at pH 7.5 appears to be relatively weak and dissociable under crystallization conditions at pH 5. Since the maximal activity of DyPs, including DyP2, is typically found below pH 5,[16,18−20] it is unclear whether the monomer, oligomer, or an equilibrium mixture represents the physiological form.

The overall α/β ferredoxin-like fold of the DyP2 protomer is shared with other structurally characterized DyPs[16,21,24] but differs in the arrangements of loops and α-helices that surround the β-barrel core (Figure 4B,C). These loops appear to also create a deeper active site pocket in DyP2 (Figure 4BC, Supplementary Figure S14) compared to the bacterial DypB from *R. jostii* RHA1, which has been suggested to be the origin of high peroxidase activity of the C- and D-type DyPs against a wide range of substrates.[21] The active site of DyP2 shows that the heme is ligated to H321 as the proximal residue with the conserved Arg (R346) and Asp (D190) in the distal pocket (Figure 4D), which mutational studies have shown to be important for DyP peroxidase activity.[16,40] In addition, the distal heme pocket contains an ambiguous oxygen species (Supplementary Figure S15). On the basis of the resolution of the data, this electron density has been assigned to a single mobile water molecule. However, the elongated density in this region of both the $2F_o-F_c$ and the F_o-F_c maps leave the possibility that a diatomic oxygen adduct with an O−O distance of 1.3 Å may be present in the active site instead (Supplementary Figure S15).

The most striking feature of the DyP2 crystal structure is the existence of a bound Mn ion in a binding site formed by E258, E273, E284, and a structured water held in place by a hydrogen bond to the main chain carbonyl of E273 (Figure 4D). Although the final DyP2 model does not show the E273 side chain to be coordinated to the Mn ion, the electron density maps indicate that it is fluxional and that a second conformation where the carboxylic acid moiety is directly ligated to the Mn ion also exists (Supplementary Figure S16). This binding site does not appear to be common among DyPs based on sequence analysis and appears to be limited to a handful of other C-type DyPs (Supplementary Figure S17). However, peroxidases from other families have been shown or predicted to contain Mn binding sites. For example, the crystal structure of the MnP from *P. chrysosporium* shows a Mn ion to be coordinated by three carboxylates, one heme propionate, and two waters.[41] The versatile peroxidases from *Pleurotus eryngii* have been shown to have a Mn binding site similar to that of the MnP.[42] Although the Mn site in DyP2 shows fluxionality, the $K_M(Mn^{2+})$ of DyP2 is only 10-fold higher than that of MnP. Indeed, the versatile peroxidase from *P. eryngii* also may share this fluxionality in the coordination of one of the glutamate side chains to the Mn and demonstrates the same affinity for Mn^{2+} as MnP.[42] We also find a potential redox-active amino acid (Y188) in between the heme and Mn pocket that could serve to communicate between these sites, which are separated by 15 Å. Overall, the existence of a distinct binding site for Mn demonstrates that the Mn-dependent behavior of DyP2 both as a peroxidase and oxidase likely plays a key role in its catalytic function.

Conclusions. In summary, we have identified and characterized DyP2 from *A.* sp. 75iv2 and found that it is a versatile and multifunctional member of the DyP family. As a peroxidase, it demonstrates high activity against a broad range of peroxidase substrates, including the high-potential Reactive Black 5. In addition, DyP2 demonstrates Mn peroxidase activity near the same order of magnitude as canonical Mn peroxidases and versatile peroxidases that are involved in fungal pathways for lignin breakdown and take advantage of the high Mn content of wood and other plant material. The observed high activity differs from other characterized bacterial DyPs but is consistent with its unusual phylogeny shared with DyPs from related actinomycetes that demonstrate the capacity to depolymerize biomass. DyP2 also demonstrates a second

mode of oxidase reactivity that was predicted for the MsP1 and MsP2 DyPs[17] but may be more mechanistically complex than canonical oxidases given its Fe^{3+} resting state. Interestingly, the oxidase mode is also dependent on Mn^{2+}, with a similar $K_M(Mn^{2+})$ as the Mn peroxidase activity, and broadens its substrate scope to include more challenging substrates. Crystallographic studies show that a distinct Mn binding site exists and indicate that Mn has an essential physiological role in DyP2 function.

METHODS

Bacterial Strains. *E. coli* DH10B-T1^R and BL21(de3)-T1^R were used for plasmid construction and heterologous protein production, respectively. *A.* sp. 75iv2 ATCC 39116 was purchased from the American Tissue Type Collection.

Plasmid Construction. The gene encoding DyP2 was amplified from *A.* sp. 75iv2 genomic DNA and inserted into the NdeI-HindIII sites of pCWOri-HisN. The resulting construct was verified by sequencing (Quintara Biosciences).

Phylogenetic Analysis and Sequence Alignments. Representative DyP sequences were identified from the four known DyP clades by searching the Uniprot database[43] using sequences of each of the structurally characterized members with UniRef50 to yield homologues with <50% sequence identity. Of these DyPs, 10−12 sequences were chosen from each clade for analysis. To increase the breadth of C-clade DyPs, an additional 13 *A.* sp. 75iv2 DyP2 homologues were identified using BLAST[44] and included in the sequence alignment. A structure-based alignment was generated from these sequences using Expresso[45] on the T-COFFEE Multiple Sequence Alignment Server.[46] The alignment output was then analyzed with MEGA 5.0[47] using a maximum likelihood statistical method with a nearest-neighbor-interchange strategy, while allowing for deletion of gaps that exist in <50% of the sequences. The confidence was evaluated with 500 bootstraps.

Purification of His_{10}-DyP2 and Selenomethione-Labeled His_{10}-DyP2. Unlabeled His_{10}-DyP2 was expressed overnight in *E. coli* BL21(de3) at 25 °C in TB containing carbenicillin (Cb, 50 μg mL^{-1}). For production of selenomethione-labeled His_{10}-DyP2, cultures were first grown in LB Cb, washed with MOPS-M9, and supplemented with an amino acid mixture including selenomethionine before overnight induction at 25 °C. α-Aminolevulinic acid (65 μg mL^{-1}) was added at the time of induction for both unlabeled and labeled enzyme. Cell pellets were harvested by centrifugation at 9,800 × *g* for 7 min and stored at −80 °C. Frozen cell pellets were thawed and resuspended with 50 mM potassium phosphate, 300 mM sodium chloride, 10 mM imidazole, pH 8.0 containing PMSF (0.5 mM), DTT (1 mM), and DNase (2 U g^{-1} cell paste). The cell paste was homogenized before lysis by passage through a French Pressure cell (Thermo Scientific) at 14,000 psi. The lysate was centrifuged at 15,300 × *g* for 30 min at 4 °C to remove insoluble material. His_{10}-DyP2 was purified from the soluble fraction on an ÄKTApurifier FPLC (GE Healthcare Life Sciences) using a Ni-NTA agarose column (Qiagen). After concentration, the Ni-NTA eluate was further purified by size exclusion chromatography using a HiLoad 16/20 Superdex 200 prep grade size exclusion chromatography column (GE Healthcare Life Sciences). To remove bound imidazole, the protein was then dialyzed to a 10^{-6} final dilution of the original buffer. The extinction coefficient of His_{10}-DyP2 (unlabeled, R_z = 1.6−1.8; SeMet-labeled, R_z = 2.02) at 280 nm was measured to be 61,800 M^{-1} cm^{-1} by protein acidolysis (AAA Service Laboratory). The protein (~25 mg L^{-1} final yield) was stored at −80 °C after addition of glycerol (10% (v/v) final concentration).

ICP-OES Analysis. His_{10}-DyP2 was analyzed for Fe content using standard protocol.[12] From this analysis, the extinction coefficient of the Soret band for His_{10}-DyP2 was determined to be 113,300 M^{-1} cm^{-1} at 404 nm. Based on the Fe content and concentration measured by analysis, the heme loading of His_{10}-DyP2 was determined to be >99%.

Dynamic Light Scattering Analysis. Dynamic light scattering data (n = 20) was collected for His_{10}-DyP2 (0.5 mg mL^{-1}) on a DynaPro Titan (Wyatt Technology Corporation) at 589 nm and 25 °C over a 1 s interval. ASTRA was used to analyze and average the data using a Raleigh spheres model to obtain the hydrodynamic radius and particle diameter.

Redox Potential Determination. The Fe^{II}/Fe^{III} couple of His_{10}-DyP2 was measured anaerobically both by spectrochemical and spectroelectrochemical titration in the presence of a redox mediator cocktail. Spectrochemical titration was carried out using literature protocol[48] with a modified cell. The spectroelectrochemical titration was carried out in a semimicro quartz magnetic stir cell (Starna Cells) with a platinum gauze working electrode, platinum counter electrode, and Ag/AgCl reference electrode. The BASi Epsilon potentiostat was set to −550 mV *vs* Ag/AgCl to reduce His_{10}-DyP2 and increased stepwise to −150 mV *vs* Ag/AgCl, allowing each potential to stabilize for 1 h. For spectrochemical titrations, His_{10}-DyP2 was analyzed using oxidation-reduction potential and Ag/AgCl reference microelectrodes (Microelectrodes, Inc.). After initial reduction with dithionite, ODQ (0.5 mM) was titrated in to oxidize His_{10}-DyP2. The reaction was allowed to equilibrate for 45 min after each addition. UV−vis spectra were collected at each potential on an Agilent 8453 diode-array spectrophotometer equipped with an Agilent 8909A stirring module. The fraction of reduced DyP2 was monitored by $\Delta A_{560\ nm}$ and used to determine the midpoint reduction potential.[49]

Crystallization and Structure Determination of His_{10}-DyP2. Protein crystals were obtained using the hanging drop vapor diffusion method by combining equal volumes of protein solution (6−7 mg mL^{-1}) and reservoir solution containing 0.1 M sodium acetate, pH 4.9−5.2, $MnCl_2$ (22 mM), and poly(ethylene glycol) 4000 (8.0−8.5%). The crystals were cryoprotected by briefly soaking in 3:1 (v/v) well solution/ethylene glycol. Data were collected at Beamline 8.3.1 at the Advanced Light Source (Lawrence Berkeley National Laboratory) and processed using the XDS[50] and CCP4[51] software packages with 5% of the reflections flagged for R_{free} calculations. Phases were determined by a combination of a partial molecular replacement solution using *B. adusta* Dec1 DyP (PDB ID 2D3Q) as search model and the location of the selenium atoms determined by SAD using Phaser[52] and a 3.0 Å resolution data set from a SeMet-His_{10}-DyP2 crystal. Electron density maps were improved by density modification and noncrystallographic symmetry averaging using Parrot[53] before building the initial model using Buccaneer.[54] The final model was then generated through multiple rounds of manual building in COOT[55] and refinement using the PHENIX package[56] using 2.25 Å resolution data from a His_{10}-DyP2 crystal.

Spectrophotometric Activity Assays. All assays were performed at 25 °C using a Beckman DU-800 spectrophotometer. Data are reported as the mean ± SE (n = 3−6) as determined from curve fitting. Error in the k_{cat}/K_M parameter was obtained from propagation of error from the individual kinetic terms. 2,4-dichlorophenol, Reactive Blue 5, ABTS, and Reactive Black 5 oxidation were assayed by modified literature protocols with H_2O_2 (0.5 mM) in 50 mM sodium acetate at pH 4.5. Mn^{2+} oxidation was assayed with H_2O_2 (0.5 mM) in 50 mM sodium malonate at pH 4.5. The pH-rate profile for Reactive Blue 5 was collected with a variation of Britton and Robinson buffers as previously described.[12]

HPLC Assay for Monitoring Peroxide-Dependent Degradation of Lignin Model Compounds. Lignin model dimers, guaiacylglycerol-β-guaiacol ether (**1**) and veratrylglycerol-β-guaiacol ether (**2**), were prepared as previously reported[12] to test reactivity of DyP2. Reactions (1 mL) were performed in 50 mM sodium acetate, pH 4.5 containing H_2O_2 (1 mM) and lignin model compounds (1 mM) and initiated with addition of His_{10}-DyP2 (0.2 μM). When added, $MnCl_2$ was supplemented to a final concentration of 1 mM. All reactions were allowed to stir overnight at RT. The solution was centrifuged at 20,817 × *g* for 5 min to remove any particulate matter, and the cleared solution was analyzed by reverse-phase HPLC.

Assays for Monitoring DyP2 Oxidase Activity. DyP2 oxidase reactivity was assayed using a modified literature assay for oxidative decarboxylation of MMA to anisaldehyde.[36] Reactions were performed

in 50 mM sodium acetate, pH 4.5 containing H_2O_2 (1 mM), $MnCl_2$ (5 mM), and MMA (2.5 mM), initiated with addition of His_{10}-DyP2 (0.1 μM), and analyzed by reverse-phase HPLC. For the boiled protein control, His_{10}-DyP2 was incubated at 100 °C for 15 min to denature protein before adding to the assay mixture. Anaerobic controls were set up in an anaerobic glove-box (Plas Laboratories) and quenched by boiling before exposing to air. To verify the identity of the product, the reaction mixture was also analyzed by GC−MS and compared to an anisaldehyde standard.

Complete Materials and Methods. Detailed procedures can be found in the Supporting Information.

■ ASSOCIATED CONTENT

Ⓢ Supporting Information

Full description of experimental materials and methods, phylogenetic and bioinformatic analysis, crystallization and refinement statistics, structural analysis, and biochemical characterization. This material is available free of charge via the Internet at http://pubs.acs.org.

Accession Codes

The atomic coordinates and structure factors for the DyP2 structure reported herein have been deposited in the Protein Data Bank as entry 4G2C.

■ AUTHOR INFORMATION

Corresponding Author

*E-mail: mcchang@berkeley.edu.

Notes

The authors declare no competing financial interest.

■ ACKNOWLEDGMENTS

This work was funded by the generous support of the Energy Biosciences Institute (OO0J06). M.E.B. acknowledges the John Stauffer Fund for a predoctoral fellowship, and T.B. acknowledges EMBO for a Long-term Fellowship (ALTF 576-2009). We thank J. Holton (Beamline 8.3.1, Advanced Light Source, Lawrence Berkeley National Laboratory) for helpful discussions on X-ray data collection and analysis, Q. Wang for assistance with DLS experiments, and J. Jurss for help with spectroelectrochemical titrations.

■ REFERENCES

(1) Claassen, P. A. M., van Lier, J. B., Lopez Contreras, A. M., van Niel, E. W. J., Sijtsma, L., Stams, A. J. M., de Vries, S. S., and Weusthuis, R. A. (1999) Utilization of biomass for the supply of energy carriers. *Appl. Microbiol. Biotechnol. 52*, 741−755.

(2) Greene, N. (2004) *Growing energy: How biofuels can help end America's oil dependence*, Natural Resources Defense Council, New York.

(3) Himmel, M. E., Ding, S.-Y., Johnson, D. K., Adney, W. S., Nimlos, M. R., Brady, J. W., and Foust, T. D. (2007) Biomass recalcitrance: Engineering plants and enzymes for biofuels production. *Science 315*, 804−807.

(4) Langeveld, J. W. A., Dixon, J., and Jaworski, J. F. (2010) Development perspectives of the biobased economy: A review. *Crop Sci. 50*, S142−S151.

(5) Ralph, J., Lundquist, K., Brunow, G., Lu, F., Kim, H., Schatz, P. F., Marita, J. M., Hatfield, R. D., Ralph, S. A., Christensen, J. H., and Boerjan, W. (2004) Lignins: Natural polymers from oxidative coupling of 4-hydroxylphenylpropanoids. *Phytochem. Rev. 3*, 29−60.

(6) Kirk, T. K., and Farrell, R. L. (1987) Enzymatic "combustion": The microbial degradation of lignin. *Annu. Rev. Microbiol. 41*, 465−505.

(7) ten Have, R., and Teunissen, P. J. (2001) Oxidative mechanisms involved in lignin degradation by white-rot fungi. *Chem. Rev. 101*, 3397−3413.

(8) Ramachandra, M., Crawford, D. L., and Hertel, G. (1988) Characterization of an extracellular lignin peroxidase of the lignocellulolytic actinomycete *Streptomyces viridosporus*. *Appl. Environ. Microbiol. 54*, 3057−3063.

(9) Kirby, R. (2005) Actinomycetes and lignin degradation, in *Advances in Applied Microbiology* (Laskin, A. I., Bennett, J. W., Gadd, G. M., and Sariaslani, S., Eds.) pp 125−168, Academic Press, London, U.K.

(10) Ahmad, M., Taylor, C. R., Pink, D., Burton, K., Eastwood, D., Bending, G. D., and Bugg, T. D. H. (2010) Development of novel assays for lignin degradation: Comparative analysis of bacterial and fungal lignin degraders. *Mol. BioSyst. 6*, 815−821.

(11) Crawford, D. L., Pometto, A. L., III, and Crawford, R. L. (1983) Lignin degradation by *Streptomyces viridosporus*: Isolation and characterization of a new polymeric lignin degradation intermediate. *Appl. Environ. Microbiol. 45*, 898−904.

(12) Brown, M. E., Walker, M. C., Nakashige, T. G., Iavarone, A. T., and Chang, M. C. Y. (2011) Discovery and characterization of heme enzymes from unsequenced bacteria: Application to microbial lignin degradation. *J. Am. Chem. Soc. 133*, 18006−18009.

(13) Davis, J. R., Goodwin, L. A., Woyke, T., Teshima, Hazuki, Bruce, D., Detter, C., Tapia, R., Han, S., Han, J., Pitluck, S., Nolan, M., Mikhailova, N., Land, M. L., and Sello, J. K. (2012) Genome sequence of *A.* sp. strain ATCC 39116, a plant biomass-degrading actinomycete. *J. Bacteriol. 194*, 2396−2397.

(14) Sugano, Y. (2009) DyP-type peroxidases comprise a novel heme peroxidase family. *Cell. Mol. Life Sci. 66*, 1387−1403.

(15) Johjima, T., Ohkuma, M., and Kudo, T. (2003) Isolation and cDNA cloning of novel hydrogen peroxide-dependent phenol oxidase from the basidiomycete *Termitomyces albuminosus*. *Appl. Microbiol. Biotechnol. 61*, 220−225.

(16) Sugano, Y., Muramatsu, R., Ichiyanagi, A., Sato, T., and Shoda, M. (2007) DyP, a unique dye-decolorizing peroxidase, represents a novel heme peroxidase family. *J. Biol. Chem. 282*, 36652−36658.

(17) Scheibner, M., Hülsdau, B., Zelena, K., Nimtz, M., de Boer, L., Berger, R., and Zorn, H. (2008) Novel peroxidases of *Marasmius scorodonius* degrade β-carotene. *Appl. Microbiol. Biotechnol. 77*, 1241−1250.

(18) Ogola, H. J. O., Kamiike, T., Hashimoto, N., Ashida, H., Ishikawa, T., Shibata, H., and Sawa, Y. (2009) Molecular characterization of a novel peroxidase from the cyanobacterium *Anabaena* sp. Strain PCC 7120. *Appl. Environ. Microbiol. 75*, 7509−7518.

(19) Liers, C., Bobeth, C., Pecyna, M., Ullrich, R., and Hofrichter, M. (2010) DyP-like peroxidases of the jelly fungus *Auricularia auricula-judae* oxidize nonphenolic lignin model compounds and high-redox potential dyes. *Appl. Microbiol. Biotechnol. 85*, 1869−1879.

(20) Li, J., Liu, C., Li, B., Yuan, H., Yang, J., and Zheng, B. (2012) Identification and molecular characterization of a novel DyP-type peroxidase from *Pseudomonas aeruginosa* PKE117. *Appl. Biochem. Biotechnol. 166*, 774−785.

(21) Roberts, J. N., Singh, R., Grigg, J. C., Murphy, M. E. P., Bugg, T. D. H., and Eltis, L. D. (2011) Characterization of dye-decolorizing peroxidases from *Rhodococcus jostii* RHA1. *Biochemistry 50*, 5108−5119.

(22) Ahmad, M., Roberts, J. N., Hardiman, E. M., Singh, R., Eltis, L. D., and Bugg, T. D. H. (2011) Identification of DypB from *Rhodococcus jostii* RHA1 as a lignin peroxidase. *Biochemistry 50*, 5096−5107.

(23) Kim, S. J., and Shoda, M. (1999) Purification and characterization of a novel peroxidase from *Geotrichum candidum* Dec 1 involved in decolorization of dyes. *Appl. Environ. Microbiol. 65*, 1029−1035.

(24) Zubieta, C., Krishna, S. S., Kapoor, M., Kozbial, P., McMullan, D., Axelrod, H. L., Miller, M. D., Abdubek, P., Ambing, E., Astakhova, T., Carlton, D., Chiu, H.-J., Clayton, T., Deller, M. C., Duan, L., Elsliger, M.-A., Feuerhelm, J., Grzechnik, S. K., Hale, J., Hampton, E.,

Han, G. W., Jaroszewski, L., Jin, K. K., Klock, H. E., Knuth, M. W., Kumar, A., Marciano, D., Morse, A. T., Nigoghossian, E., Okach, L., Oommachen, S., Reyes, R., Rife, C. L., Schimmel, P., van den Bedem, H., Weekes, D., White, A., Xu, Q., Hodgson, K. O., Wooley, J., Deacon, A. M., Godzik, A., Lesley, S. A., and Wilson, I. A. (2007) Crystal structures of two novel dye-decolorizing peroxidases reveal a β-barrel fold with a conserved heme-binding motif. *Proteins: Struct., Funct., Bioinf. 69*, 223−233.

(25) Sato, T., Hara, S., Matsui, T., Sazaki, G., Saijo, S., Ganbe, T., Tanaka, N., Sugano, Y., and Shoda, M. (2004) A unique dye-decolorizing peroxidase, DyP, from *Thanatephorus cucumeris* Dec 1: Heterologous expression, crystallization and preliminary X-ray analysis. *Acta Crystallogr., Sect. D 60*, 149−152.

(26) Battistuzzi, G., Bellei, M., Bortolotti, C. A., and Sola, M. (2010) Redox properties of heme peroxidases. *Arch. Biochem. Biophys. 500*, 21−36.

(27) Sugano, Y., Matsushima, Y., and Shoda, M. (2006) Complete decolorization of the anthraquinone dye Reactive Blue 5 by the concerted action of two peroxidases from *Thanatephorus cucumeris* Dec 1. *Appl. Microbiol. Biotechnol. 73*, 862−871.

(28) Heinfling, A., Ruiz-Dueñas, F. J., Martínez, M. J., Bergbauer, M., Szewzyk, U., and Martínez, A. T. (1998) A study on reducing substrates of manganese-oxidizing peroxidases from *Pleurotus eryngii* and *Bjerkandera adusta*. *FEBS Lett. 428*, 141−146.

(29) Zubieta, C., Joseph, R., Krishna, S. S., McMullan, D., Kapoor, M., Axelrod, H. L., Miller, M. D., Abdubek, P., Acosta, C., Astakhova, T., Carlton, D., Chiu, H.-J., Clayton, T., Deller, M. C., Duan, L., Elias, Y., Elsliger, M.-A., Feuerhelm, J., Grzechnik, S. K., Hale, J., Han, G. W., Jaroszewski, L., Jin, K. K., Klock, H. E., Knuth, M. W., Kozbial, P., Kumar, A., Marciano, D., Morse, A. T., Murphy, K. D., Nigoghossian, E., Okach, L., Oommachen, S., Reyes, R., Rife, C. L., Schimmel, P., Trout, C. V., van den Bedem, H., Weekes, D., White, A., Xu, Q., Hodgson, K. O., Wooley, J., Deacon, A. M., Godzik, A., Lesley, S. A., and Wilson, I. A. (2007) Identification and structural characterization of heme binding in a novel dye-decolorizing peroxidase, TyrA. *Proteins: Struct., Funct., Bioinf. 69*, 234−243.

(30) Fernández-Fueyo, E., Ruiz-Dueñas, F. J., Miki, Y., Martínez, M. J., Hammel, K. E., and Martínez, A. T. (2012) Lignin-degrading peroxidases from genome of selective ligninolytic fungus *Ceriporiopsis subvermispora*. *J. Biol. Chem. 287*, 16903−16916.

(31) Kuan, I. C., Johnson, K. A., and Tien, M. (1993) Kinetic analysis of manganese peroxidase. The reaction with manganese complexes. *J. Biol. Chem. 268*, 20064−20070.

(32) Banci, L., Camarero, S., Martínez, A., Martínez, M., Pérez-Boada, M., Pierattelli, R., and Ruiz-Dueñas, F. (2003) NMR study of manganese(II) binding by a new versatile peroxidase from the white-rot fungus *Pleurotus eryngii*. *J. Biol. Inorg. Chem. 8*, 751−760.

(33) Katayama, T., Nakatsubo, F., and Higuchi, T. (1981) Syntheses of arylglycerol-β-aryl ethers. *Mokuzai Gakkaishi 27*, 223−230.

(34) Wei, K., Luo, S.-W., Fu, Y., Liu, L., and Guo, Q.-X. (2004) A theoretical study on bond dissociation energies and oxidation potentials of monolignols. *J. Mol. Struct.: THEOCHEM 712*, 197−205.

(35) Tien, M., and Ma, D. (1997) Oxidation of 4-methoxymandelic acid by lignin peroxidase. *J. Biol. Chem. 272*, 8912−8917.

(36) Baciocchi, E., Gerini, M. F., Lanzalunga, O., and Mancinelli, S. (2002) Lignin peroxidase catalysed oxidation of 4-methoxymandelic acid. The role of mediator structure. *Tetrahedron 58*, 8087−8093.

(37) Yamazaki, I., and Piette, L. H. (1963) The mechanism of aerobic oxidase reaction catalyzed by peroxidase. *Biochim. Biophys. Acta 77*, 47−64.

(38) Paszczynski, A., Huynh, V.-B., and Crawford, R. (1986) Comparison of ligninase-I and peroxidase-M2 from the white-rot fungus *Phanerochaete chrysosporium*. *Arch. Biochem. Biophys. 244*, 750−765.

(39) Krissinel, E., and Henrick, K. (2007) Inference of macromolecular assemblies from crystalline state. *J. Mol. Biol. 372*, 774−797.

(40) Singh, R., Grigg, J. C., Armstrong, Z., Murphy, M. E. P., and Eltis, L. D. (2012) Distal heme pocket residues of B-type dye-decolorizing peroxidase: Arginine but not aspartate is essential for peroxidase activity. *J. Biol. Chem. 287*, 10623−10630.

(41) Sundaramoorthy, M., Youngs, H., Gold, M. H., and Poulos, T. L. (2005) High-resolution crystal structure of manganese peroxidase: Substrate and inhibitor complexes. *Biochemistry 44*, 6463−6470.

(42) Pérez-Boada, M., Ruiz-Dueñas, F. J., Pogni, R., Basosi, R., Choinowski, T., Martínez, M. J., Piontek, K., and Martínez, A. T. (2005) Versatile peroxidase oxidation of high redox potential aromatic compounds: Site-directed mutagenesis, spectroscopic and crystallographic investigation of three long-range electron transfer pathways. *J. Mol. Biol. 354*, 385−402.

(43) The UniProt Consortium (2012) Reorganizing the protein space at the Universal Protein Resource (UniProt). *Nucleic Acids Res. 40*, D71−D75.

(44) Altschul, S. F., Madden, T. L., Schäffer, A. A., Zhang, J., Zhang, Z., Miller, W., and Lipman, D. J. (1997) Gapped BLAST and PSI-BLAST: A new generation of protein database search programs. *Nucleic Acids Res. 25*, 3389−3402.

(45) Armougom, F., Moretti, S., Poirot, O., Audic, S., Dumas, P., Schaeli, B., Keduas, V., and Notredame, C. (2006) Expresso: Automatic incorporation of structural information in multiple sequence alignments using 3D-Coffee. *Nucleic Acids Res. 34*, W604−W608.

(46) Notredame, C., Higgins, D. G., and Heringa, J. (2000) T-coffee: A novel method for fast and accurate multiple sequence alignment. *J. Mol. Biol. 302*, 205−217.

(47) Tamura, K., Peterson, D., Peterson, N., Stecher, G., Nei, M., and Kumar, S. (2011) MEGA5: Molecular evolutionary genetics analysis using maximum likelihood, evolutionary distance, and maximum parsimony methods. *Mol. Biol. Evol. 28*, 2731−2739.

(48) Makino, R., Park, S.-y., Obayashi, E., Iizuka, T., Hori, H., and Shiro, Y. (2011) Oxygen binding and redox properties of the heme in soluble guanylate cyclase. *J. Biol. Chem. 286*, 15678−15687.

(49) Dutton, P. L. (1978) Redox potentiometry: Determination of midpoint potentials of oxidation-reduction components of biological electron-transfer systems. *Methods Enzymol. 54*, 411−435.

(50) Kabsch, W. (2010) XDS. *Acta Crystallogr., Sect. D 66*, 125−132.

(51) Collaborative Computational Project No. 4 (1994) The CCP4 suite: Programs for protein crystallography, *Acta Crystallogr., Sect. D 50*, 760−763.

(52) McCoy, A. J., Grosse-Kunstleve, R. W., Adams, P. D., Winn, M. D., Storoni, L. C., and Read, R. J. (2007) Phaser crystallographic software. *J. Appl. Crystallogr. 40*, 658−674.

(53) Zhang, K. Y. J., Cowtan, K., and Main, P. (1997) Combining constraints for electron-density modification. *Methods Enzymol. 277*, 53−64.

(54) Winn, M. D., Ballard, C. C., Cowtan, K. D., Dodson, E. J., Emsley, P., Evans, P. R., Keegan, R. M., Krissinel, E. B., Leslie, A. G. W., McCoy, A., McNicholas, S. J., Murshudov, G. N., Pannu, N. S., Potterton, E. A., Powell, H. R., Read, R. J., Vagin, A., and Wilson, K. S. (2011) Overview of the CCP4 suite and current developments. *Acta Crystallogr., Sect. D 67*, 235−242.

(55) Emsley, P., and Cowtan, K. (2004) Coot: Model-building tools for molecular graphics. *Acta Crystallogr., Sect. D 60*, 2126−2132.

(56) Adams, P. D., Afonine, P. V., Bunkoczi, G., Chen, V. B., Davis, I. W., Echols, N., Headd, J. J., Hung, L.-W., Kapral, G. J., Grosse-Kunstleve, R. W., McCoy, A. J., Moriarty, N. W., Oeffner, R., Read, R. J., Richardson, D. C., Richardson, J. S., Terwilliger, T. C., and Zwart, P. H. (2010) PHENIX: A comprehensive Python-based system for macromolecular structure solution. *Acta Crystallogr., Sect. D 66*, 213−221.